The first *in-silico* model of leg movement activity during sleep

Matteo Italia*[1], Andrea Danani[2], Fabio Dercole[1], Raffaele Ferri[3], Mauro Manconi[4]

[1] Department of Electronics, Information, and Bioengineering, Politecnico di Milano, Milan, Italy (matteo.italia@polimi.it and fabio.dercole@polimi.it)

[2] Dalle Molle Institute for Artificial Intelligence, University of Southern Switzerland, University of Applied Sciences and Arts of Southern Switzerland, Lugano Universitary Center, Lugano, Switzerland (andrea.danani@idsia.ch)

[3] Oasi Research Institute – IRCCS, Troina, Italy (rferri@oasi.en.it)

[4]Sleep Medicine Unit, Neurocenter of Southern Switzerland, Ospedale Civico, Lugano. Faculty of Biomedical Sciences, Università della Svizzera Italiana, Lugano, Switzerland. Department of Neurology, University Hospital, Inselspital, Bern, Switzerland (mauro.manconi@eoc.ch)

*corresponding author

Keywords: leg movement activity, periodic leg movements, restless legs syndrome.

Abstract. We developed the first model simulator of leg movements activity during sleep. We designed and calibrated a phenomenological model on control subjects not showing significant periodic leg movements (PLM). To test a single generator hypothesis behind PLM—a single pacemaker possibly resulting from two (or more) interacting spinal/supraspinal generators—we added a periodic excitatory input to the control model. We describe the onset of a movement in one leg as the firing of a neuron integrating physiological excitatory and inhibitory inputs from the central nervous system, while the duration of the movement was drawn in accordance with statistical evidence. The period and the intensity of the periodic input were calibrated on a dataset of subjects showing PLM (mainly restless legs syndrome patients). Despite its many simplifying assumptions—the strongest being the stationarity of the neural processes during night sleep—the model simulations are in remarkably agreement with the polysomnographically recorded data.

1 Scientific Background

Leg movement activity (LMA) during sleep refers to all tibialis anterior muscle activity events of one leg compliant with onset, offset, and amplitude criteria set by the World Association of Sleep Medicine (WASM) [1]. LMA is detected by recording both tibialis anterior muscles by means of surface electromyography in the context of polysomnography. Periodic leg movements (PLM) are particular involuntary LMA, typically occurring during sleep (PLMS). PLM are a frequent phenomenon present in the majority of patients with restless legs syndrome (RLS), in a significant percentage of patients with other sleep disorders, and even in healthy subjects especially elderly [2, 3].

Based on WASM criteria, PLM consist of series of at least four monolateral or bilateral candidate leg movements (CLM), each of them longer than 0.5 and shorter than 10 s (or 15 s for bilateral movements) and separated by 10-90 s. When two left and right movements overlap or are separated by less than 0.5 s they are considered as one bilateral leg movement; otherwise as two distinct monolateral movements [1]. The severity of PLM is quantified by the PLM index, indicating the PLM number per hour, and considered abnormal, by consensus, when it exceeds the value of 15 during sleep [4].

PLM might affect sleep quality for their association with cortical arousals and, in the long term, cardiovascular system, because of the repetitive induced increase of heart rate and blood pressure [5]. However, the mechanism and the neuroanatomic pathways behind PLM are largely unknown, as well as the origin of their periodicity. PLMS also occur in patients with complete transverse lesions indicating that the spinal cord contains the fundamental network to generate them [6, 7]. In particular, since PLM might occur in one or both legs, one unsolved question is whether the network is generating one or two excitatory rythms (pacemakers).

The model is calibrated on data from both control and PLM subjects (subjects with significant/abnormal PLM index, in particular RLS patients). It allows to generate populations of virtual subjects, both control and PLM, and to simulate *in-silico* LMA. This goes beyond a speculative exercise: besides understanding the PLM cause, it has potential implications for the clinical practice, in particular on the essential decision to treat PLMs or not [8]. Indeed, this work is the first step in developing an *in-silico* laboratory that can bring tremendous benefits to doctors and patients, e.g., including pharmacological effects to investigate the fundamental decision to treat or not PLM, and, in case, how to optimally treat PLM. Moreover, a mathematical *in-silico* LMA model has indisputable advantages with respect to animal models, from both the ethical and economic viewpoints [9].

This work is a preliminary and modeling oriented version of the article recently appeared in the *Journal of Sleep Research* [10].

2 Materials and Methods

2.1 The LMA model

We drastically simplify the underlying physiology (Fig. 1 shows a schematic representation and an example of *in-silico* LMA) and assume that each leg is controlled by a single motor neuron (circular nodes in the figure), representative of the central nervous system complex pathways ultimately determining contractions of the leg muscles. The two neurons are modeled with the well-known Stein integrate-and-fire (IF) model [11] (see [12] for a review).

The IF mechanism is quite simple. The neuron state is characterized by its membrane potential (middle in Fig. 1), which evolves according to the neuron synaptic inputs. Excitatory (E)/inhibitory (I) inputs (bottom panel in Fig. 1) increase/decrease the membrane potential (middle panel in Fig. 1), while a time constant τ rules the potential discharge toward a resting value V_0. When the potential reaches a fire threshold V_{th}, an output spike is generated, which causes the potential to reset at a basal value that we take, for simplicity, to be the resting value V_0. The output spike represents, in our model, the leg movement onset, while the duration of the movement is drawn from a distribution fitted on clinical data (see next section and the top panel in Fig. 1). We neglect the neuron refractory period, i.e., after firing the neuron immediately restarts integrating inputs (firing in the course of a LM is a rare event in our model, $\leq 3\%$, and are disregarded with no significant effect on our results).

Each of the two neurons receive E/I inputs from the physiological activity of the central nervous systems, a proportion p of which equally affect both legs, while the remaining fraction $(1-p)$ is leg-specific (see the rectangles and their firing rates in Fig. 1). For subjects showing significant PLM (subject typically characterized by a bimodal distribution of the intermovement interval (IMI) and by a large PLM index), we add a periodic input common to both legs that implements our hypothesis of a single phenomenological PLM pacemaker (brown PLM generator in Fig. 1). The period and intensity of the periodic input are patient-specific.

We model the physiological inputs as series of synaptic current spikes, with Poissonian arrival times, each causing the membrane potential to instantaneously step by a

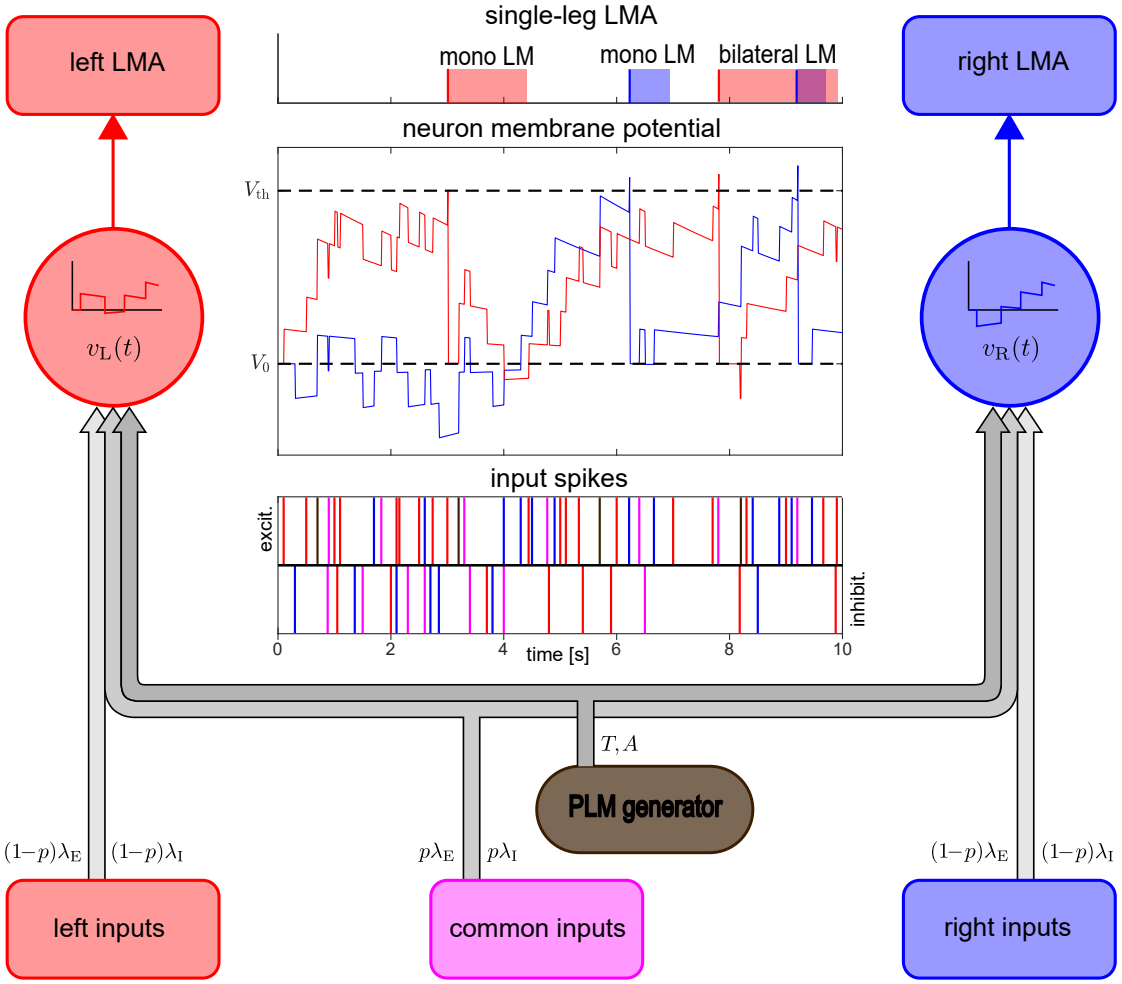

Figure 1: Schematic representation of the model together with an example of *in-silico* LMA generation. The left and right motor neurons (red and blue circular nodes) implement the Stein integrate-and-fire model, with membrane potentials $v_{\rm L}(t)$ and $v_{\rm R}(t)$ at time t and the same rest potential V_0 and fire threshold $V_{\rm th}$ (see eq. (1)). Leg specific and common physiological inputs from the central nervous systems (red, blue, and magenta rectangular source nodes) are modeled by spikes of synaptic current with Poissonian arrival times causing steps of equal amplitude a in the membrane potentials (positive/negative steps for excitatory/inhibitory spikes; arrival rates are indicated next to the input arrow). The assumed single PLM generator (brown) produces a periodic train of excitatory spikes with period T and potential step amplitude A. Example of simulated LMA: given the input spikes (stochastically drawn in accordance with their arrival rates), the left/right neuron membrane potential evolves according to eq. (1); when the neuron fires, an LM starts on its controlled leg, with duration drawn from a data-fitted distribution (see model calibration Sect. 2.2). Single-leg LMA are combined in monolateral and bilateral LM according to the standard rule [1]: two monolateral and one bilateral LM are shown in the top panel.

small fraction a of the rest-to-fire interval $V_{\text{th}} - V_0$. We denote by λ_{E} and λ_{I} the arrival rates of E and I inputs, divided into common (rate $p\,\lambda_{\text{X}}$) and leg-specific (same rate $(1-p)\,\lambda_{\text{X}}$ for both legs, X = E, I) (lower part of Fig. 1). The three Poisson arrival processes (common and left-/right-specific) are independent. The PLM pacemaker is a series of T-periodic synaptic spikes, each spike causing an upward potential step A.

Denoting by $v_{\text{l}}(t)$ and $v_{\text{r}}(t)$ the left and right neurons membrane potential at time t (red and blue curve in Fig. 1 middle panel), their time evolution is ruled by the following ordinary differential equation:

$$\frac{d}{dt}v_{\text{x}}(t) = -\frac{v_{\text{x}}(t) - V_0}{\tau} + a\,S_{\text{E}}(t) + a\,S_{\text{E,x}}(t) - a\,S_{\text{I}}(t) - a\,S_{\text{I,x}}(t) + A\,S_{\text{P}}(t), \quad (1)$$

x = l, r, where $S_{\text{E}}(t)$, $S_{\text{E,x}}(t)$, $S_{\text{I}}(t)$, and $S_{\text{I,x}}(t)$ are the series of unitary spikes of the physiological inputs (common to both legs and leg-specific), and $S_{\text{P}}(t)$ is the periodic series of unitary spikes of the PLM pacemaker (a unitary spike causing a 1-Volt upward step in the membrane potential). Between two consecutive inputs, the potential $v_{\text{x}}(t)$ exponentially decays toward V_0 (the evolution is only ruled by the discharge term in eq. (1)). At the arrival of the new input spike, the potential is updated by adding the spike contribution.

2.2 Model calibration

Data were obtained from subjects previously enrolled in different studies on PLM published by some of the authors of this work (M.M. and R.F.) [6, 13, 14]. The LMA duration is fitted on all control LMA recordings (32 subjects characterized by unimodal IMI distribution; max PLM index = 5.9; mean age 48.03 years (SD 20.75) and 56.25% women). Parameters λ_{E}, λ_{I}, p, τ characterize control subjects. Their calibration result is a statistical fitting that can be used to generate virtual control subjects populations. The distributions of the PLM generator parameters T and A are fitted using the PLM dataset (65 subjects, mainly RLS affected, characterized by bimodal IMI distribution; PLM index > 15 except for a few cases; mean age 58.52 years (SD 13.09) and 66.15% women). All parameters are supposed constant during the night (8 hours). All calibration procedures are implemented in Matlab. Fig. 2 shows the results for the control model. The calibration result of the PLM generator parameters is shown in Fig. 3. More details on the calibration follow.

2.2.1 Scaling parameters

From a phenomenological standpoint, the membrane potential rest and threshold values, V_0 and V_{th}, are scaling parameters. We set $V_0 = 0$ and $V_{\text{th}} = 1$ and express the intensities a and A of the physiological and pathological synaptic inputs as fractions of the rest-to-fire interval (V_0, V_{th}, a, and A can therefore be considered adimensional). In particular, the intensity a played a scaling role affecting the calibration of the arrival rates λ_{E} and λ_{I}. With no loss of generality, we fixed $a = 0.1$ ($(V_{\text{th}} - V_0)/10$), i.e., one-tenth of the rest-to-fire interval.

2.2.2 LMA duration

We collected the durations of all LMAs recorded on each single leg in the control dataset. We fitted the obtained LMA samples with all parametric distributions provided in Matlab. None however showed statistical agreement with the LMA data (Kolmogorov-Smirnov test (K-S) p-value < 0.01). We then used a non-parametric technique [15] (kernel density estimation, mean 2.47, SD 2.43, Fig. 2A; K-S p-value ≈ 0.15) and used the obtained distribution to independently draw the durations of all

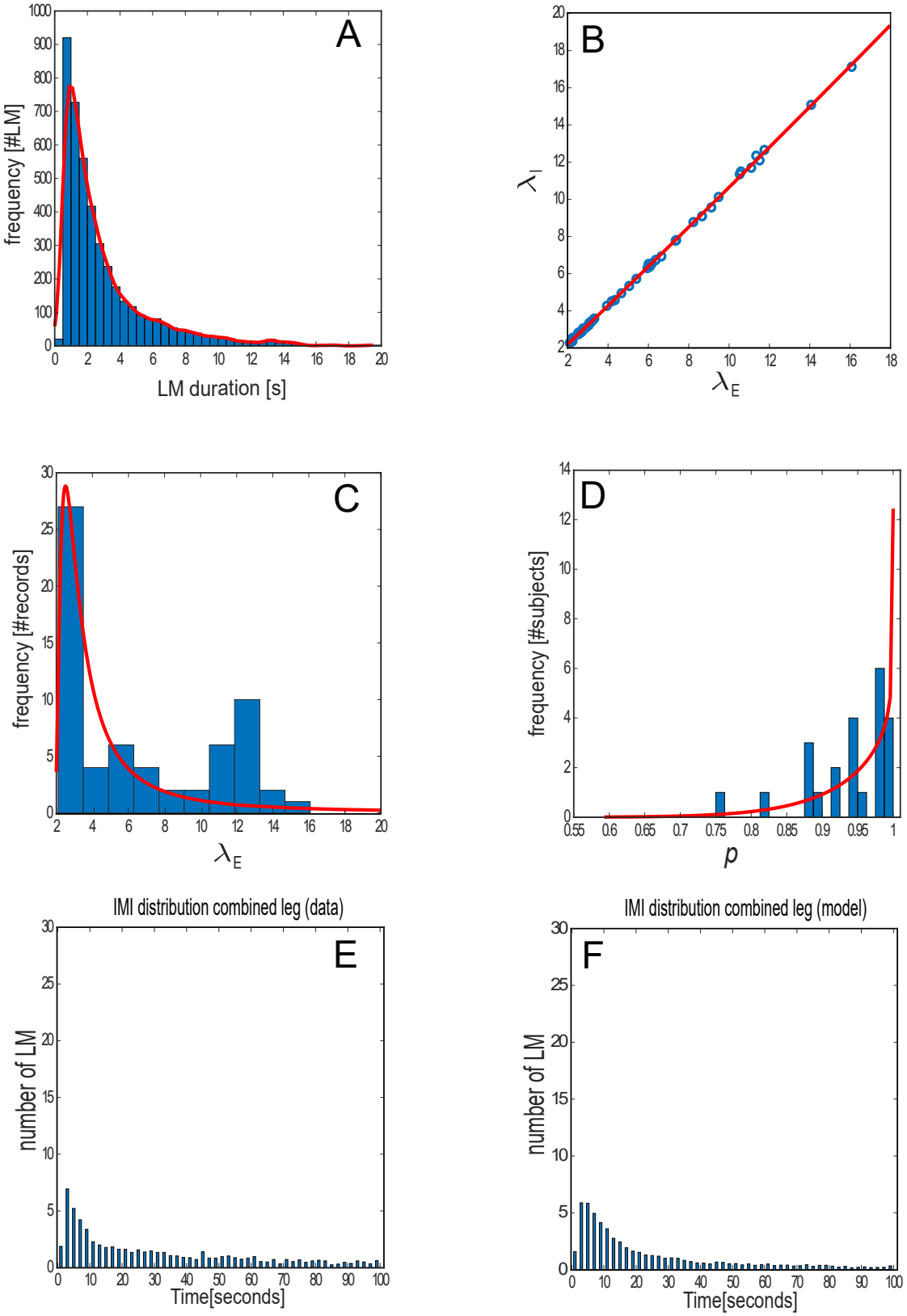

Figure 2: Samples histograms (blue) and fitted distributions (red line) of LMA duration (A), E inputs arrival rate λ_E (B), common/specific proportion parameter p (D). (λ_I, λ_E) correlation (C).
IMI distribution of the population of real (E) and virtual (F) control subjects.

virtual LMA at the firing of the corresponding leg neuron. Because no significant correlation is documented between LMA duration and subject's PLM index, we use the LMA duration distribution fitted on controls also to generate the LMA of virtual PLM subjects.

2.2.3 Arrival rates of physiological input spikes

We jointly calibrated the arrival rates of the physiological input spikes on single leg recordings of the control subjects. Not distinguishing common from leg-specific inputs, E and I spikes arrive at rate λ_{E} and λ_{I} on each single leg, independently on the value of the proportion parameter p. The membrane time constant τ, however, affects the calibration of λ_{E} and λ_{I}. We now describe the calibration for an assigned value of τ.

For each single leg recording, we added to the sample joint distribution of $(\lambda_{\mathrm{E}}, \lambda_{\mathrm{I}})$ the pair that matches the observed mean and variance of the IMI. Note that we considered the intervals between all LMA (recall that a leg activity shorter than 0.5 s is not scored as LM [1]), because our model aims at reproducing the full LMA. As the difference $\lambda_{\mathrm{E}} - \lambda_{\mathrm{I}}$ and the sum $\lambda_{\mathrm{E}} + \lambda_{\mathrm{I}}$ respectively controlled the IMI mean and variance of a virtual control subject [12], we adjusted them to match the observed values over a one-night simulation (accuracy 5%). As we found a strong correlation between λ_{E} and λ_{I}, we chose to fit the sample distribution of λ_{E} and a relation binding λ_{I} to λ_{E}.

For the selected value $\tau = 75$ s (see section below 2.2.5), we found a nearly-linear correlation between λ_{E} and λ_{I} that we fitted with the least-square-error quadratic polynomial with the addition of a small Gaussian term to account for the data variability (the variance of the Gaussian was set equal to the polynomial square error). We obtained $\lambda_{\mathrm{I}} = 1.031\lambda_{\mathrm{E}} + 0.1187 + 0.002136\lambda_{\mathrm{E}}^2 + 0.05\,N(0,1)$ and we best fitted λ_{E} to the generalized extreme value (GEV) (3.10, 1.22, 0.89) (Fig. 2B-C). To avoid unrealistic values, we truncated the obtained GEV at $\lambda_{\mathrm{E}} = 20$ (truncated GEV mean 4.73, SD 3.14; K-S p-value ≈ 0.3).

2.2.4 Proportion of common and leg-specific inputs

For assigned τ, λ_{E}, λ_{I}, we built the sample distribution of the proportion parameter p between common and leg-specific physiological inputs as follows. For each control subject, we obtained a sample of p by matching the proportion of bilateral LMs shown by the subject with the one produced by the virtual subject characterized by rates λ_{E} and λ_{I} equal to the corresponding averages of the values identified for the subject's left and right legs. At each value of p during the search (we used bisection from the two extremes $p = 0$ and $p = 1$, with accuracy 3%), we simulated 10 nights of the virtual subject and compared the obtained fraction of bilateral LMs with the value shown by the real subject. The obtained samples of p are fitted with all common parametric distributions. The best parametric distribution fit for $\tau = 75$ s was the Beta (11.82, 0.82) (Fig. 2D; K-S p-value ≈ 0.71).

2.2.5 The membrane time constant

We calibrated the membrane time constant τ to match the shape of the IMI distribution of control subjects. Note that, thanks to the τ-dependent calibration of the input arrival rates λ_{E} and λ_{I} and of the common/specific proportion parameter p, the mean and variance of the IMI distribution of a virtual population well matched the experimental values, independently of τ. However, if τ was too small, the neuron discharge was too fast, so that firing required a burst of E inputs. This resulted in large input rates λ_{E} and λ_{I} and in a quite erratic dynamics of the neuron potentials, thus yielding a rather flat IMI distribution for the virtual population.

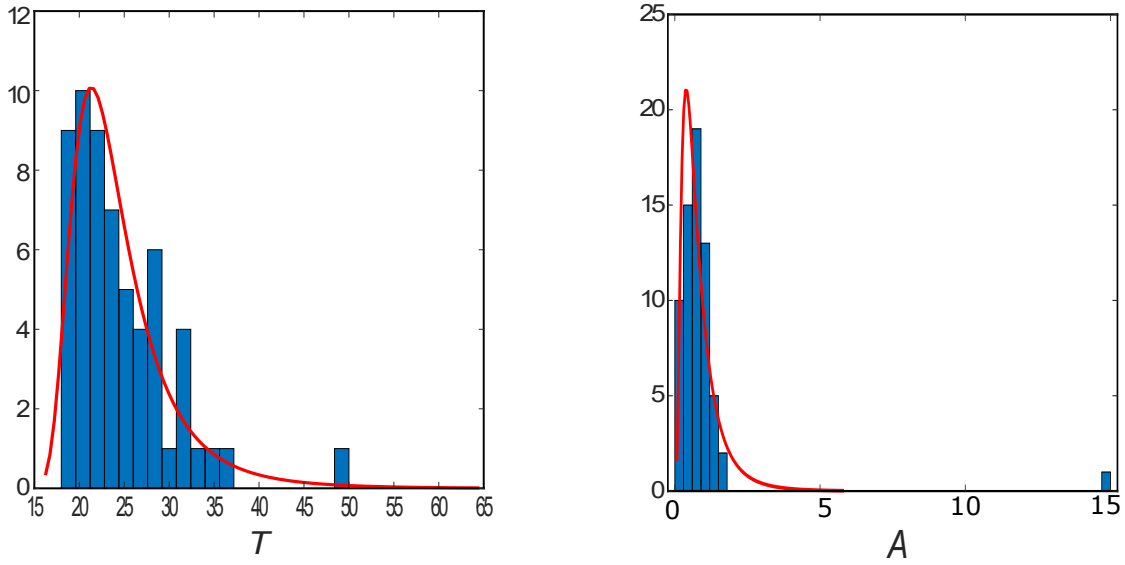

Figure 3: Samples histograms (blue) and fitted distributions (red line) of the PLM generator period T (on the panel left) and of the PLM generator intensity A (on the right panel).

Since the characteristic IMI of control subjects is in the interval 0.5-10 s, we considered, as shape index, the ratio between the hourly number of IMI < 10 s, averaged over the population, and the average LMA index (the hourly number of LMA). The reason for considering the LMA index in the ratio, instead of the total hourly number of IMI, was that the input arrival rates were calibrated to match the subject LMA.

Summarizing, to evaluate a specific value of τ, we proceeded as follows: calibrate the distribution of λ_{E} and fit its correlation with λ_{I}; calibrate the distribution of p; generate a population of 100 virtual controls; simulate one night for each control and compute the IMI distribution shape index of the virtual population. As expected, the shape index increased with τ and got close to the experimental value (20%) at about $\tau = 75$. Fig. 2E, F show the IMI distribution of real and simulated control populations, respectively.

2.2.6 The period of the PLM generator

We relied on the fact that patients with significant PLM are characterized by a bimodal IMI distribution, where the first peak is typical of healthy subjects, while the second characterizes the PLM disorder [16]. We therefore built the sample distribution of the period T by taking the IMI of the second peak of each PLM subject's IMI distribution. We found the best fitting with the GEV (21.87, 3.49, 0.17) (left panel of Fig. 3; K-S p-value ≈ 0.55). Relaying on medical experience, we truncated the GEV below 17 and above 50 s (truncated GEV mean 24.42, SD 5.16; K-S p-value ≈ 0.59).

2.2.7 The intensity of the PLM generator

For each PLM subject, we drew 10 virtual control models, to each of which we added the PLM input with the subject-specific period T and amplitude A to be selected to match the subject's LM index. PLM subjects show more LMs than control ones, so that with $A = 0$ the LM index, averaged on the 10 virtual subjects (each simulated for one night), falls below the value of the real subject. On the other extreme, if A is large, each PLM input spike triggers the firing of the neuron and the LM index of the virtual subjects exceeds the clinical value. We proceed via bisection to find the sample of A matching the subject's LM index (with accuracy of 3 movements/hr). We best fitted the LogNormal (0.78, 0.8) (K-S p-value ≈ 0.31; right panel of Fig. 3). To avoid unrealistic virtual PLM subjects, we truncated the distribution below 0.2 (truncated LogNormal mean 0.72, SD 0.60; K-S p-value ≈ 0.3).

Table 1: LM features in real (recording) and virtual (simulation) control subjects.
Statistical agreement: T, Student's t-test; Tl, t-test on log-transformed data; U, Mann–Whitney U test.

	control subjects (32)		
	recording	**simulation**	**statistics**
LM features	**mean (SD)**	**mean (SD)**	**p-value**
LMA index	13.57 (±6.34)	13.74 (±6.45)	0.8804 (T)
LM index	13.44 (±6.29)	13.54 (±6.38)	0.9289 (T)
CLM index	12.88 (±5.58)	13.00 (±6.12)	0.9040 (T)
old PLM index	5.11 (±3.51)	4.34 (±1.48)	0.3611 (U)
PLM index	1.54 (±1.59)	0.65 (±0.73)	0.0193 (U)
short-IMI index	2.71 (±2.15)	2.84 (±1.66)	0.4684 (U)
mid-IMI index	4.89 (±2.71)	4.40 (±2.34)	0.6576 (U)
long-IMI index	4.56 (±1.75)	5.02 (±1.70)	0.4051 (U)
monolateral LMs	**median (IQR)**	**median (IQR)**	**p-value**
dunuration (s), min	0.53 (0.51-0.57)	0.52 (0.51-0.55)	0.9998 (T)
max	8.50 (6.42-9.72)	8.69 (7.53-9.29)	0.6255 (T)
mean	2.01 (1.76-2.28)	2.08 (1.93-2.21)	0.3178 (T)
median	1.59 (1.29-1.70)	1.54 (1.46-1.69)	0.4118 (T)
bilateral LMs	**median (IQR)**	**median (IQR)**	**p-value**
# single LM, min	2.0 (2.00-2.00)	2.0 (2.00-2.00)	-
max	3.0 (2.00-3.00)	3.0 (2.00-3.00)	0.9158 (U)
mean	2.05 (2.00-2.11)	2.04 (2.00-2.10)	0.9561 (U)
median	2.0 (2.00-2.00)	2.0 (2.00-2.00)	-
duration (s), min	1.01 (0.82-1.13)	0.96 (0.81-1.22)	0.4573 (T)
max	9.19 (8.26-9.69)	9.67 (8.37-11.82)	0.0531 (T)
mean	3.91 (3.52-4.35)	4.09 (3.57-4.59)	0.2346 (T)
median	3.34 (2.98-3.91)	3.28 (2.85-3.74)	0.4109 (T)
bilateral LMs (%)	31.45 (23.50-40.00)	30.94 (15.45)	0.8505 (T)

3 Results and Discussion

Our model can be used to generate *in-silico* populations of both control and PLM subjects. We create populations of equal size to the datasets used for the model calibration (32 control and 65 PLM subjects) and compare the obtained sample distributions of typical clinical indicators against polysomnographically-recorded data. A limitation of this study is that we use for the comparison the same datasets used for calibration. On one hand, the datasets are too small to be split into calibration and validation. Moreover, the model parameters show a remarkable variability among the subjects, so that a correct validation would require more recordings of the same subjects. On the other hand, our model does not simulate the specific parameter values identified for single real subjects, but randomly draw virtual subjects from the statistics of the real control and PLM populations. Finally, the model is not aimed at forecasting the LMA of new subjects. Our primary aim in this work is to test the single-generator hypothesis behind PLM. For these reasons, it is acceptable to use the same dataset for calibration and assessment.

In calibration, we have identified the distributions of the model parameters that best fit the LMA of control and PLM subjects. In validation, we compare important features of virtual populations drawn from the identified statistics against the real populations.

Table 2: LM features in real (recording) and virtual (simulation) PLM subjects.
Statistical agreement: T, Student's t-test; Tl, t-test on log-transformed data; U, Mann–Whitney U test.

	PLM subjects (65)		
	recording	**simulation**	**statistics**
LM features	**mean (SD)**	**mean (SD)**	**p-value**
LMA index	57.12 ($\pm$46.40)	61.36 ($\pm$45.48)	0.2436 (Tl)
LM index	56.90 ($\pm$46.22)	60.69 ($\pm$45.15)	0.2865 (Tl)
CLM index	55.31 ($\pm$42.67)	57.52 ($\pm$42.21)	0.5108 (Tl)
old PLM index	44.22 ($\pm$32.02)	39.48 ($\pm$41.04)	0.0749 (U)
PLM index	29.17 ($\pm$19.78)	14.21 ($\pm$22.81)	$\leq$ 0.0001 (U)
short-IMI index	12.45 ($\pm$24.69)	17.15 ($\pm$11.67)	0.2573 (U)
mid-IMI index	37.12 ($\pm$22.10)	35.08 ($\pm$31.61)	0.3899 (U)
long-IMI index	4.05 ($\pm$1.76)	8.58 ($\pm$2.85)	$\leq$ 0.0001 (U)
monolateral LMs	**median (IQR)**	**median (IQR)**	**p-value**
dunuration (s), min	0.51 (0.51-0.53)	0.51 (0.51-0.52)	0.5943 (U)
max	9.30 (7.35-9.77)	9.42 (8.78-9.74)	0.5311 (U)
mean	2.15 (1.80-2.39)	2.06 (1.94-2.11)	0.3614 (U)
median	1.69 (1.40-2.14)	1.51 (1.42-1.57)	0.2269 (U)
bilateral LMs	**median (IQR)**	**median (IQR)**	**p-value**
# single LM, min	2.0 (2.00-2.00)	2.0 (2.00-2.00)	-
max	3.0 (3.00-4.00)	4.0 (3.00-4.00)	0.1312 (U)
mean	2.03 (2.01-2.06)	2.05 (2.03-2.07)	0.0973 (U)
median	2.0 (2.00-2.00)	2.0 (2.00-2.00)	-
duration (s), min	0.92 (0.73-1.10)	0.83 (0.66-0.97)	0.1153 (U)
max	9.71 (9.47-9.91)	12.99 (11.56-13.87)	$\leq$ 0.0001 (Tl)
mean	3.70 (3.34-4.31)	3.90 (3.67-4.09)	0.0502 (Tl)
median	3.32 (2.84-3.96)	3.18 (2.86-3.47)	0.1176 (Tl)
bilateral LMs (%)	39.65 (28.11-53.90)	37.63 (29.96-50.52)	0.6965 (Tl)

Table 2 summarizes the comparison, reporting mean and standard deviation of the principal LM features [13], durations, and composition of bilateral LM [14], together with their statistical agreement with real data. We find a remarkably good agreement for LMA, LM, CLM, and the old PLM indeces [1, 13] for both control and PLM populations. We also find accordance in the characteristics of monolateral and bilateral LM [14]. Noting that a virtual PLM subject is nothing but a virtual control subject with the only addition of the PLM periodic input, the latter being calibrated by fitting LMA indexes, rather than PLM indicators, we conclude that the statistical agreement gives support to the single-generator hypothesis behind the PLM phenomenon.

As expected, the agreement is strong in monolateral LM for control subjects, since the LM duration is fitted on all single-leg recordings of control subjects. Remarkably, the agreement remains very good also for the bilateral LM features validating the model for healthy subjects. Regarding PLM subjects, the obtained results support our model and thus the view of the single periodic generator. Indeed, not only the *in-silico* monolateral LM features statistically agree with the *in-vivo* ones, but also the bilateral ones, in particular the right increase of the proportion of bilateral LM in PLM subjects.

The statistical agreement fails for the indicators requiring some temporal structure among LM. This is the case of the current PLM index [1] (Tab. 2). The PLM index considers only sequences of at least four consecutive LM separated by IMI in the interval 10–90 s and interrupted by IMI shorter than 10 s or longer than 90 s. The disagreement reason is rooted in the stationarity of the model parameters during the night, especially between the various sleep phases. Indeed, without requiring sequencing, we find a good agreement in the numbers of IMI in each of the three characteristic medical interval, i.e., 0–10 s (short-IMI, characteristic of healthy individuals), 10–90 s (mid-IMI, characteristic of PLM subjects), and 90 or more seconds (long-IMI). Only the number of long-IMI is larger in our simulations, but this is again an artefact of the model stationarity. Indeed, there is medical evidence that PLM decrease along the night, i.e., mid-IMI are concentrated at the beginning of the night, while few very long IMI characterizes phases with no PLM. However, calibrating a stationary PLM generator that matches, on average, the subject's number of LM (see calibration in Sect. 2.2) gives several long-IMI in lieu of less but longer ones.

4 Conclusion

We develop the first model to generate *in-silico* LMA, both for control and PLM subjects, adding only a PLM generator for PLM subjects. We calibrate the model parameters on recorded laboratory data and simulate control and PLM virtual populations. In spite of its simplicity, our phenomenological model shows a good statistical agreement between LMA features of *in-silico* and *in-vivo* populations. The agreement supports the validity of our model and also endorses the single generator hypothesis behind the PLM phenomenon. The main dissimilarities are caused by the model stationarity, opening up for future developments aimed at turning the model into a quantitative predicting tool to support medical intervention.

It is never easy to establish the merit of a first *in-silico* model of a physiopathological phenomenon, such as LMA, and to foresee possible future useful employment. However, the interested reader can find some ideas in section 4.1 Future research in [10], where we have tried to speculate on some possible future applications of our model, such as modeling the effects of drugs.

Considering also the patients' metadata, it will be possible to perform cluster analyses for the model parameters, favoring the important and still missing mission of PLM phenotyping.

Finally, the parameters A (PLM generator intensity) and T (PLM generator period) could

be used as new indicators of the severity and temporality of PLM, respectively, to be used in parallel with the recently introduced parameters, like the periodicity index.

Acknowledgements

The authors thank the valuable suggestions received by the many reviewers. We also appreciate all the participants of the International Conference on Computational Intelligence Methods for Bioinformatics and Biostatistics, CIBB 2021, for their constructive feedback.

References

[1] R. Ferri, S. Fulda, R. Allen, M. Zucconi, O. Bruni, S. Chokroverty, L. Ferini-Strambi, B. Frauscher, D. Garcia-Borreguero, M. Hirshkowitz, B. Högl, Y. Inoue, A. Jahangir, M. Manconi, C. Marcus, D Picchietti, G. Plazzi, J.W. Winkelman, and R. Zak. "World Association of Sleep Medicine (WASM) 2016 standards for recording and scoring leg movements in polysomnograms developed by a joint task force from the International and European Restless Legs Syndrome Study Groups (IRLSSG and EURLSSG)". *Sleep Medicine*, vol.26, pp. 86-95, 2016.

[2] M. H. Pennestri, S. Whittom, B. Adam, D. Petit, J. Carrier, and J. Montplaisir "PLMS and PLMW in healthy subjects as a function of age: prevalence and interval distribution.". *Sleep*, vol.29, no.9, pp. 1183-1187, 2006.

[3] R. Ferri "The time structure of leg movement activity during sleep: the theory behind the practice". *Sleep Medicine*, vol.13, no.4, pp. 433-441, 2012.

[4] American Academy of Sleep Medicine. "International classification of sleep disorders". 2014.

[5] R. Ferri, B. Koo, D.L. Picchietti, and S. Fulda. "Periodic leg movements during sleep: phenotype, neurophysiology, and clinical significance". *Sleep Medicine*, vol.31, pp. 29-38, 2017.

[6] R. Ferri, P. Proserpio, F. Rundo, A. Lanza, K. Sambusida, T. Redaelli, F. De Carli, and L. Nobili. "Neurophysiological correlates of sleep leg movements in acute spinal cord injury". *Clinical Neurophysiology*, vol.126, no.2 , pp. 333-338, 2015.

[7] V. Salminen, M. Manconi, V. Rimpilä, T.M. Luoto, E. Koskinen, R. Ferri,J. Ohman, and 0. Polo. " Disconnection between periodic leg movements and cortical arousals in spinal cord injury". *Journal of Clinical Sleep Medicine*, vol. 9, no. 11, pp. 1207-1209, 2013.

[8] M. Figorilli, M. Puligheddu, P. Congiu, and R. Ferri. "The clinical importance of periodic leg movements in sleep". *Current Treatment Options Neurology*, vol. 19, no. 3, pp. 10, 2017.

[9] R. P. Allen, N. C. Donelson, B. C. Jones, Y. Li, M. Manconi, D. B. Rye, S. Sanyal, and J. Winkelmann. " Animal models of rls phenotypes". *Sleep Medicine*, vol. 31, pp. 23-28, 2017.

[10] M. Italia, A. Danani, F. Dercole, R. Ferri, and M. Manconi. " A calibrated model with a single-generator simulating polysomnographically recorded periodic leg movements". *Journal of Sleep Research*, Article in Press, 2022.

[11] R. B. Stein. " A theoretical analysis of neuronal variability". *Biophysical Journal*, vol. 5, no. 2, pp. 173-194, 1965.

[12] A. N. Burkitt. "A review of the integrate-and-fire neuron model: I. Homogeneous synaptic input". *Biological Cybernetics*, vol.95, pp. 1-19, 2006.

[13] R. Ferri, F. Rundo, M. Zucconi, M. Manconi, D. Aricò, O. Bruni, L. Ferini-Strambi, and S. Fulda. "Putting the periodicity back into the periodic leg movement index: an alternative data-driven algorithm for the computation of this index during sleep and wakefulness". *Sleep Medicine*, vol. 16, pp. 1229-1235, 2015.

[14] R. Ferri, M. Manconi, F. Rundo, M. Zucconi, D. Aricò, O. Bruni, F. Cosentino, L. Ferini-Strambi, and S. Fulda. "Bilateral leg movements during sleep: detailing their structure and features in normal controls and in patients with restless legs syndrome". *Sleep Medicine*, vol. 32, pp. 10-15, 2017.

[15] A. Gramacki " Nonparametric kernel density estimation and its computational aspects". Springer, 2018.

[16] R. Ferri, M. Zucconi, M. Manconi,G. Plazzi, O. Bruni, and L. Ferini-Strambi. "New approaches to the study of periodic leg movements during sleep in restless legs syndrome". *Sleep*, vol. 29, no. 6, pp. 759-769, 2006.